

A New Grid-Generation Method for 2-D Simulation of Devices with Nonplanar Semiconductor Surface

Shan-Ping Chin, *Student Member, IEEE*, and Ching-Yuan Wu, *Member, IEEE*

Abstract—A general analytical method is proposed to transform a 2-D multilayer physical domain with the nonplanar semiconductor surface into a 2-D rectangular mathematical domain with the planar surface, in which a set of Fourier series are used to describe a general conformal mapping for each layer. Based on the proposed method, a simple iteration algorithm, which incorporates a nonlinear Jacobian-iteration method with the fast-Fourier transformation (FFT), is developed to solve a system of nonlinear equations due to the mutually coupled boundary conditions. As a result of the analytical conformal mapping, a regular, deformable grid-structure can be applied to simulate the device structure with the nonplanar semiconductor surface, and the device simulator using the conventional rectangle-based grid can be easily modified to simulate the device with the nonplanar semiconductor surface.

I. INTRODUCTION

THE COMPLEXITY of device structure has been raised due to the successive improvement of device-fabrication technology. The effects of the nonplanar semiconductor surface can not be neglected for a modern scaled semiconductor device. Therefore, a device simulator with the capability of handling the nonplanar semiconductor surface is necessary for the optimal design of a scaled semiconductor device.

The basic grid-structure is very important for coding a device simulator in treating the nonplanar semiconductor surface. The triangle-based grid [1], [2] is the most widely used grid-structure in handling the nonplanar simulation domain. The major advantage of this method is its higher flexibility in locating the grid. However, this method requires more complicated codes and data structure due to the highly irregular grid-structure. Moreover, the obtuse triangle causes some problems and the efforts are needed to generate a triangular mesh without obtuse triangles.

Another approach for the grid-structure in nonplanar numerical simulation is the coordinate transformation method. This method has been widely used in other fields [3], [4] and is applied to control the quality of the grid-structure in semiconductor device simulation [5], [6]. The basic procedure of this method is that several differential

equations are described as the governing equations for coordinate transformation. A special case of coordinate transformation in 2-D simulation is that the 2-D Laplace equations are used as the governing equations. This is the well-known conformal mapping method and can be formulated by the Cauchy-Riemann relations. The single-layer numerical conformal mapping used in process simulation has been developed in [7] for treating the moving boundary problem. The major drawback of the numerical conformal mapping is that a set of 2-D Laplace equations must be solved self-consistently to satisfy the mutually coupled boundary conditions. As a result, a complicated numerical method is needed for solving these 2-D Laplace equations satisfying the mutually coupled boundary conditions.

In this paper, a simple analytical method for conformal mapping is developed, in which a set of Fourier series are used. Moreover, a curvilinear coordinate system is used to accurately describe the device structure and then is translated into the rectangular domain. The major features of this method are summarized as: 1) the regular grid structure is used to simulate the device with the nonplanar semiconductor surface; 2) the computational efforts for fitting the device structure are much reduced by adopting a nonlinear Jacobian-iteration method with the fast Fourier transformation (FFT), especially for a large number of Fourier series; 3) the discretized basic semiconductor device equations are still valid under the proposed conformal mapping.

In Section II the formulations of a general conformal mapping method are proposed and their physical pictures are discussed. In Section III a simple and efficient iteration algorithm is developed for solving a system of nonlinear equations satisfying the mutually coupled boundary conditions. Section IV shows the actual generation of the grid structure for different isolation structures in a MOS-FET and the detailed discussions on the nonlinear iteration are given. Section V gives a conclusion.

II. THE GENERAL CONFORMAL MAPPING METHOD

As shown in Fig. 1, a set of semiconductor device equations have to be solved in a physical domain $\Omega(\mu, \nu)$. The conventional 2-D semiconductor device equations can be written as:

$$\nabla^2 \Psi(\mu, \nu) = -\frac{\rho(\mu, \nu)}{\epsilon} \quad (1)$$

Manuscript received March 9, 1992; revised January 12, 1993. This work was supported by the National Science Council, Taiwan, Republic of China under Grant NSC-81-0404-E009-139. This paper was recommended by Associate Editor D. Scharfetter.

The authors are with the Advanced Semiconductor Device Research Laboratory and Institute of Electronics, National Chiao-Tung University, Hsinchu, Taiwan, Republic of China.

IEEE Log Number 9208516.

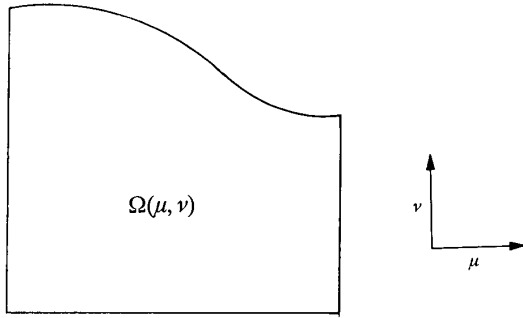


Fig. 1. The schematic cross-section of a semiconductor device with a non-planar structure.

$$\nabla \cdot (-\mu_n n \nabla \Psi + D_n \nabla n) = U_n - G_n \quad (2)$$

$$\nabla \cdot (-\mu_p p \nabla \Psi - D_p \nabla p) = U_p - G_p. \quad (3)$$

Among different grid structures, the rectangle-based grid is the most simple and widely used method in device simulation. Unfortunately, this grid-structure is limited in a rectangular-like physical domain. A transformation can be used to generalize the rectangular grid-structure to a nonplanar domain Ω . The transformation can be carried out by finding the functions $\mu_j(x, y)$ and $\nu_j(x, y)$ in each layer j . The partial differential operators under this transformation can be obtained as:

$$\frac{\partial}{\partial \mu_j} = \frac{\partial x}{\partial \mu_j} \frac{\partial}{\partial x} + \frac{\partial y}{\partial \mu_j} \frac{\partial}{\partial y}$$

and

$$\frac{\partial}{\partial \nu_j} = \frac{\partial x}{\partial \nu_j} \frac{\partial}{\partial x} + \frac{\partial y}{\partial \nu_j} \frac{\partial}{\partial y}. \quad (4)$$

Substituting (4) into (1) and (2), the Poisson's equation and the current continuity equation for electrons in the j -layer can be rewritten as

$$\begin{aligned} & \left(\frac{\partial^2 x}{\partial \mu_j^2} + \frac{\partial^2 x}{\partial \nu_j^2} \right) \frac{\partial \Psi}{\partial x} + \left(\frac{\partial^2 y}{\partial \mu_j^2} + \frac{\partial^2 y}{\partial \nu_j^2} \right) \frac{\partial \Psi}{\partial y} + \left[\left(\frac{\partial x}{\partial \mu_j} \right)^2 \right. \\ & \left. + \left(\frac{\partial x}{\partial \nu_j} \right)^2 \right] \frac{\partial^2 \Psi}{\partial x^2} + 2 \left(\frac{\partial x}{\partial \mu_j} \frac{\partial y}{\partial \mu_j} + \frac{\partial x}{\partial \nu_j} \frac{\partial y}{\partial \nu_j} \right) \\ & \cdot \frac{\partial^2 \Psi}{\partial x \partial y} + \left[\left(\frac{\partial y}{\partial \mu_j} \right)^2 + \left(\frac{\partial y}{\partial \nu_j} \right)^2 \right] \frac{\partial^2 \Psi}{\partial y^2} \\ & = -\frac{\rho(x, y)}{\epsilon} \end{aligned} \quad (5)$$

$$\begin{aligned} & \left(\frac{\partial^2 x}{\partial \mu_j^2} + \frac{\partial^2 x}{\partial \nu_j^2} \right) \left(D_n \frac{\partial n}{\partial x} - \mu_n n \frac{\partial \Psi}{\partial x} \right) + \left(\frac{\partial^2 y}{\partial \mu_j^2} + \frac{\partial^2 y}{\partial \nu_j^2} \right) \left(D_n \frac{\partial n}{\partial y} - \mu_n n \frac{\partial \Psi}{\partial y} \right) + \left[\left(\frac{\partial x}{\partial \mu_j} \right)^2 + \left(\frac{\partial x}{\partial \nu_j} \right)^2 \right] \\ & \cdot \left[\frac{\partial}{\partial x} \left(D_n \frac{\partial n}{\partial x} - \mu_n n \frac{\partial \Psi}{\partial x} \right) \right] + \left(\frac{\partial x}{\partial \mu_j} \frac{\partial y}{\partial \mu_j} + \frac{\partial x}{\partial \nu_j} \frac{\partial y}{\partial \nu_j} \right) \left[\frac{\partial}{\partial y} \left(D_n \frac{\partial n}{\partial x} - \mu_n n \frac{\partial \Psi}{\partial x} \right) + \frac{\partial}{\partial x} \left(D_n \frac{\partial n}{\partial y} - \mu_n n \frac{\partial \Psi}{\partial y} \right) \right] \\ & + \left[\left(\frac{\partial y}{\partial \mu_j} \right)^2 + \left(\frac{\partial y}{\partial \nu_j} \right)^2 \right] \left[\frac{\partial}{\partial y} \left(D_n \frac{\partial n}{\partial y} - \mu_n n \frac{\partial \Psi}{\partial y} \right) \right] = U_n - G_n. \end{aligned} \quad (6)$$

Similar treatment can be applied to the continuity equation for holes.

There are many pairs of the functions $\mu(x, y)$ and $\nu(x, y)$ that can be used to define a general transformation. However, the above equations are too complicated in a general coordinate transformation and must be further simplified by applying the following constraint equations:

$$\frac{\partial x}{\partial \mu_j} \frac{\partial y}{\partial \mu_j} + \frac{\partial x}{\partial \nu_j} \frac{\partial y}{\partial \nu_j} = 0 \quad (7a)$$

$$\left(\frac{\partial x}{\partial \mu_j} \right)^2 + \left(\frac{\partial x}{\partial \nu_j} \right)^2 = \left(\frac{\partial y}{\partial \mu_j} \right)^2 + \left(\frac{\partial y}{\partial \nu_j} \right)^2. \quad (7b)$$

The constraint function (7a) is used to preserve the right angle between the lines in the transformation. For instance, the lines $\mu(x, y)$ and $\nu(x, y)$ for $x = \text{constant}$ and $y = \text{constant}$ constitute an orthogonal curvilinear coordinate system. Note that the corners in the simulation domain are limited to the right angle by the constraint due to the right angle of the mathematical plane. The constraint function (7b) means the conservation of the aspect ratio of an infinite small cell, i.e.,

$$\frac{\int_x^{x+dx} [(\partial \mu / \partial x)^2 + (\partial \nu / \partial x)^2]^{1/2} dx}{\int_y^{y+dy} [(\partial \mu / \partial y)^2 + (\partial \nu / \partial y)^2]^{1/2} dy} = \frac{dx}{dy}. \quad (8)$$

As a result, the transformation produces the changes of position and size but keeps the angle and the aspect ratio under the constraints of (7a) and (7b). An example showing the transformation from a rectangular finite-box to a deformable finite-box under these constraints is plotted in Fig. 2. It is clearly seen that the orthogonality between the grid lines is preserved.

Although (7a) and (7b) are seen to be nonlinear, however, the linearized forms of (7a) and (7b) can be expressed as the well-known Cauchy-Riemann relations for the 2-D case:

$$\frac{\partial x}{\partial \mu_j} = \frac{\partial y}{\partial \nu_j} \quad \text{and} \quad \frac{\partial x}{\partial \nu_j} = -\frac{\partial y}{\partial \mu_j}. \quad (9)$$

From (9), we obtain

$$\frac{\partial^2 x}{\partial \mu_j^2} + \frac{\partial^2 x}{\partial \nu_j^2} = 0 \quad \text{and} \quad \frac{\partial^2 y}{\partial \mu_j^2} + \frac{\partial^2 y}{\partial \nu_j^2} = 0. \quad (10)$$

Note that the first and second terms in (5) and (6) become vanished if the 2-D Laplace equations in (10) are used.

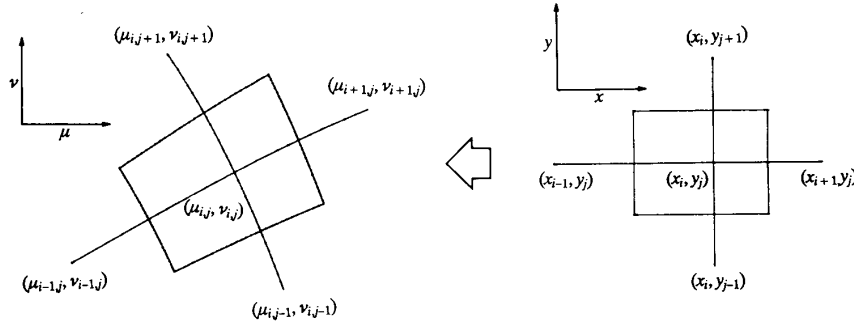


Fig. 2. An example showing the mapping of a finite-box from the $x - y$ (mathematical) plane onto the $\mu - \nu$ (physical) plane.

The relations in (9) are also true for their inverse functions:

$$\frac{\partial \mu_j}{\partial x} = \frac{\partial \nu_j}{\partial y} \quad \text{and} \quad \frac{\partial \mu_j}{\partial y} = -\frac{\partial \nu_j}{\partial x}. \quad (11)$$

From (7a), (7b), and (10), the 2-D Poisson's equation and the 2-D current continuity equations defined in the mathematical $x - y$ plane can be rewritten as

$$\frac{\partial^2 \Psi}{\partial x^2} + \frac{\partial^2 \Psi}{\partial y^2} = -J \frac{\rho(x, y)}{\epsilon} \quad (12)$$

$$\frac{\partial}{\partial x} \left(D_n \frac{\partial n}{\partial x} - \mu_n n \frac{\partial \Psi}{\partial x} \right) + \frac{\partial}{\partial y} \left(D_n \frac{\partial n}{\partial y} - \mu_n n \frac{\partial \Psi}{\partial y} \right) = J(U_n - G_n), \quad (13)$$

where $J = [(\partial x / \partial \mu_j)^2 + (\partial y / \partial \nu_j)^2]^{-1}$. Note that (12) and (13) show a fact that the basic semiconductor equations are invariant under the transformation satisfied by the Cauchy-Riemann relations. It is interesting to note that the discretized semiconductor device equations are not changed after the transformation from a rectangular domain to a nonplanar domain if the transformation is conformal. The invariability of the angle between the conjugate grid lines and the aspect ratio of the finite box is very useful in modifying the codes used for simulating the planar device structure to those for simulating the nonplanar device structure.

In order to find a set of the conjugate functions, $\mu_j(x, y)$ and $\nu_j(x, y)$, satisfied (11) in each layer, the equations in (11) can be decoupled by mutual substitution, and the resulting equations can be written as a set of 2-D Laplace equations:

$$\frac{\partial^2 \mu_j}{\partial x^2} + \frac{\partial^2 \mu_j}{\partial y^2} = 0 \quad \text{and} \quad \frac{\partial^2 \nu_j}{\partial x^2} + \frac{\partial^2 \nu_j}{\partial y^2} = 0. \quad (14)$$

Although the 2-D Laplace equations in (14) form a set of decoupled linear equations, it must be noted that the boundary conditions of these two Laplace equations are mutually coupled. As shown in Fig. 3, the numerical domain ($x - y$) is mapped to the physical domain ($\mu - \nu$), and the boundary conditions for (14) must satisfy the

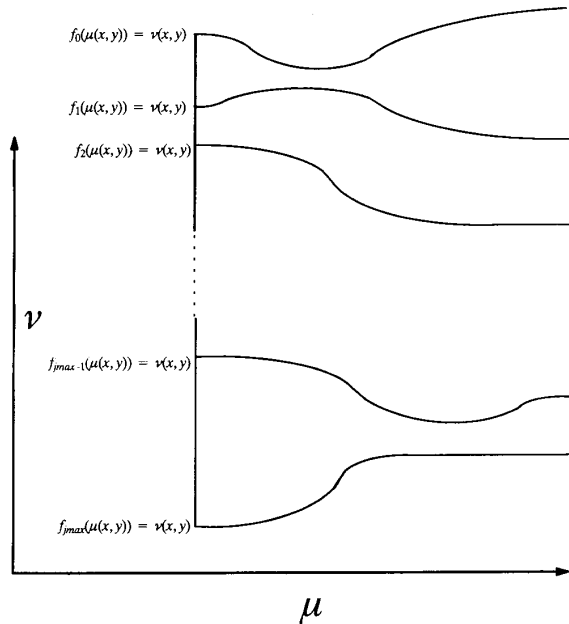


Fig. 3. An example showing the relation between the device structure and the mutually coupled boundary condition.

shape of the device structure in each layer, i.e.,

$$f_j(\mu(x, y_j)) = \nu(x, y_j), \quad \text{for } j = 0, 1, 2, \dots, j_{\max}, \quad (15)$$

where j and j_{\max} denote the j th interface and the total number of the layer to be fitted, respectively.

The coupled boundary conditions in (15) describe the nonlinear equations due to the shape of the semiconductor device and need a numerical algorithm to get the solution of (15). A numerical method for solving the above 2-D partial differential equations with mutually coupled boundary conditions can be found in [7]. However, the numerical method for getting a conformal mapping needs much computational efforts due to a large linear system with mutually coupled boundary conditions. The problem for doing this coordinate transformation analytically is how to get a set of general solutions for (11). Our ap-

proach is based on a set of Fourier cosine series with eigenvalue k_m ($= m\pi/L$):

$$\begin{aligned} \mu_j(x, y) = x + \sum_{m=1}^{\infty} \frac{\sin(k_m x)}{\sinh(k_m b_j)} [A_{j,m} \cosh k_m \\ \cdot (b_j - y + y_j) + B_{j,m} \cosh k_m (y - y_j)] \end{aligned} \quad (16a)$$

$$\begin{aligned} \nu_j(x, y) = y - y_j - \sum_{m=1}^{\infty} \frac{\cos(k_m x)}{\sinh(k_m b_j)} [A_{j,m} \sinh k_m \\ \cdot (b_j - y + y_j) - B_{j,m} \sinh k_m (y - y_j)]. \end{aligned} \quad (16b)$$

Note that the conjugate functions, $\mu_j(x, y)$ and $\nu_j(x, y)$ in (16), are the particular solutions of the 2-D Laplace equations in (14), respectively. The coefficients, $A_{j,m}$ and $B_{j,m}$, have to be solved by satisfying mutually coupled boundary conditions (15).

Substituting (16a) and (16b) into (15), the following equations can be obtained for $y = y_j$ and $y = y_j + b_j$:

$$\begin{aligned} f_j \left(x + \sum_{m=1}^{\infty} \sin(k_m x) [A_{j,m} \coth(k_m b_j) \right. \\ \left. + B_{j,m} \operatorname{csch}(k_m b_j)] \right) \\ = - \sum_{m=1}^{\infty} A_{j,m} \cos(k_m x), \end{aligned} \quad (17a)$$

$$\begin{aligned} f_{j+1} \left(x + \sum_{m=1}^{\infty} \sin(k_m x) [A_{j,m} \operatorname{csch}(k_m b_j) \right. \\ \left. + B_{j,m} \coth(k_m b_j)] \right) \\ = b_j + \sum_{m=1}^{\infty} B_{j,m} \cos(k_m x). \end{aligned} \quad (17b)$$

Transforming (17a) and (17b) into cosine-Fourier series, the following equations are obtained:

$$f_{j,m} = -A_{j,m}, \quad \text{for } m = 1, 2, 3, \dots, \infty \quad (18a)$$

$$f_{j+1,m} = B_{j,m}, \quad \text{for } m = 1, 2, 3, \dots, \infty \quad (18b)$$

$$b_j = f_{j+1,0} - f_{j,0} \quad (18c)$$

where $f_{j,m}$ and $f_{j+1,m}$ are the Fourier coefficients of $f_j(\mu(x, y_j))$ and $f_{j+1}(\mu(x, y_j + b_j))$, respectively, and can be expressed as:

$$\begin{aligned} f_{j,m} = \frac{c}{L} \int_0^L f_j(\mu(x, y_j)) \cos(k_m x) dx, \\ c = 1 \text{ for } m = 0; c = 2 \text{ for } m \neq 0 \end{aligned} \quad (19a)$$

$$\begin{aligned} f_{j+1,m} = \frac{c}{L} \int_0^L f_{j+1}(\mu(x, y_j + b_j)) \cos(k_m x) dx, \\ c = 1 \text{ for } m = 0; c = 2 \text{ for } m \neq 0. \end{aligned} \quad (19b)$$

The mutually coupled boundary conditions have been transformed into a system of nonlinear equations (18a)–(18c). The algorithm for solving these coefficients will be presented in Section III.

III. NUMERICAL ALGORITHM

As pointed out in the previous section, an iterative method is required for obtaining the coefficients A_m and B_m . These coefficients must be determined from the known device structure. The computation efficiency and accuracy for solving (18a)–(18c) are determined by two factors: one is the number of Fourier series; the other is the numerical method and its convergence criterion in the nonlinear iteration. The FFT method is used to perform the Fourier transformation, in which the number of Fourier series can be expressed as $n = 2^p$, where p is a positive integer. The major advantage of the FFT algorithm is that CPU time for a FFT transformation is $O(n \times \log(n))$. This feature is very important for accurately modeling the device structure with a large number of Fourier series.

Among the solution methods for a system of nonlinear equations, the Newton's method is the best known procedure. In general, the Newton's method is expected to give quadratic convergence, provided that a sufficiently accurate initial guess is needed. However, the Newton's method needs to construct a Jacobian matrix and its inversion. The CPU time for calculating the coefficient in the Jacobian matrix for the nonlinear system (18a)–(18c) is $O(n \times n \times \log(n))$ by using a FFT algorithm. As a result, the efficiency of the Newton's method will degrade seriously when the problem size is large. This limits the Newton's method to the case with only a small number of unknown variables. Thus, a nonlinear Jacobian-iteration is adopted to solve the system of nonlinear equations, which is more favorable than the Newton's method for a large problem size because the Jacobian matrix is not necessary for the proposed nonlinear Jacobian-iteration scheme. However, the major drawback of the nonlinear Jacobian iteration is that the coupling effect between the variables is not well considered and the convergence of the nonlinear Jacobian iteration is strongly dependent on the property of the equations.

The algorithm for solving the coefficients $A_{j,m}$ and $B_{j,m}$ with ω as a relaxation parameter is listed as follows:

Procedure Fourier_Conformal_Mapping

Initialize $A_{j,m}$, $B_{j,m}$, and b_j

$p = 1$

For $k = 1, k_{\max}$ **do**

Calculate $\mu_j^k(x, y_j)$ and $\mu_j^k(x, y_j + b_j)$ **by** FFT

Calculate $f_j^k(x)$ and $f_{j+1}^k(x)$

Translate $f_j^k(x)$ and $f_{j+1}^k(x)$ **To** $f_{j,m}^k$ and $f_{j+1,m}^k$ **by** FFT

$b_j^{k+1} = f_{j+1,0}^k - f_{j,0}^k$

For $m = 1, 2^p$ **do**

$A_{j,m}^{k+1} = A_{j,m}^k - \omega(f_{j,m}^k + A_{j,m}^k)$

$B_{j,m}^{k+1} = B_{j,m}^k + \omega(f_{j+1,m}^k - B_{j,m}^k)$

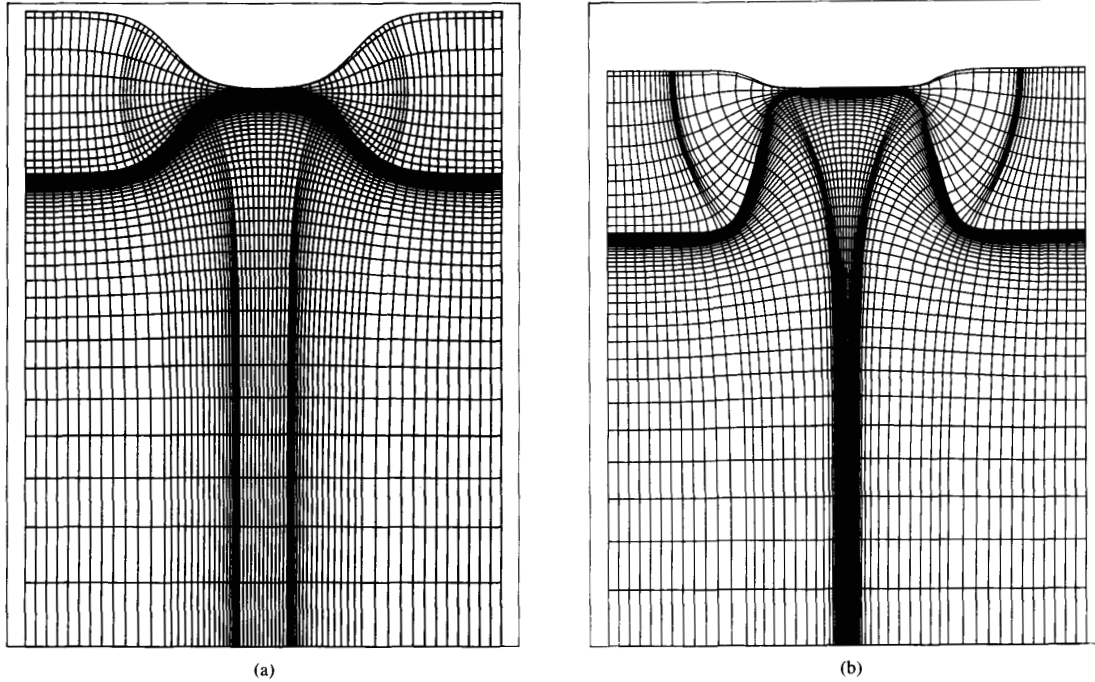


Fig. 4. The grid structures for different isolation structures: (a) LOCOS structure, and (b) Trench-like structure.

End for

If (convergence criterion is reached) **then**

$p = p + 1$

Initialize $A_{j,m} = 0, B_{j,m} = 0$ for $m = 2^{p-1} + 1$ to 2^p

Calculate increasing residue

If (increasing residue less than one half of convergence criterion) **stop**

End if

End for

End Fourier_Conformal_Mapping

where the symbol k denotes the k th iteration; n denotes the number of Fourier series, which is equal to 2^p . In this algorithm, two FFT procedures are needed for each Jacobian iteration. Note that the convergence criterion must be properly chosen to avoid the generation of the ripple-like grids.

Generally, the convergence of Fourier series is $O(e^{-n})$ for C^∞ function. This property is useful for the continuation method in solving A_m and B_m . The solutions for the problem with the 2^p terms of Fourier series are used as the initial guess for the problem with the 2^{p+1} terms of Fourier series. As the residue of the iteration for the problem with the 2^p terms of Fourier series reaches to a certain criterion, p is increased by 1. The p is increased until the truncation error of Fourier series meets the requirement of the desired accuracy. In this algorithm, the maximum number of p is determined by the increased residue less than one half of the convergence criterion when p is increased by 1. According to the convergence of Fourier

series ($O(e^{-n})$), the truncation error of Fourier series is expected to be around the residue of nonlinear iteration.

Once the coefficients A_m and B_m are determined by the numerical algorithm, the grid points in each node (i', j') can be determined by

$$\begin{aligned} \mu_{i',j'} = x_{i',j} &+ \sum_{m=1}^{\infty} \frac{\sin(k_m x_{i',j})}{\sinh(k_m b_j)} \\ &\cdot [A_{j,m} \cosh k_m (b_j - y_{j'} + y_j) + B_{j,m} \\ &\cdot \cosh k_m (y_{j'} - y_j)] \end{aligned} \quad (20a)$$

and

$$\begin{aligned} \nu_{i',j'} = y_{j'} - y_j &- \sum_{m=1}^{\infty} \frac{\cos(k_m x_{i',j})}{\sinh(k_m b_j)} \\ &\cdot [A_{j,m} \sinh k_m (b_j - y_{j'} + y_j) - B_{j,m} \\ &\cdot \sinh k_m (y_{j'} - y_j)]. \end{aligned} \quad (20b)$$

Note that the coefficients A_m and B_m are different for each subdomain and the x -grid lines in each mathematical subdomain must be determined to meet the continuity of μ -grid lines across the interface between the subdomain.

IV. RESULTS AND DISCUSSIONS

In this section, some practical examples showing the applications of the proposed Fourier conformal mapping algorithm are demonstrated and discussed in detail. The generated grid structures for comparing the narrow-width effect between different isolation structures: LOCOS and

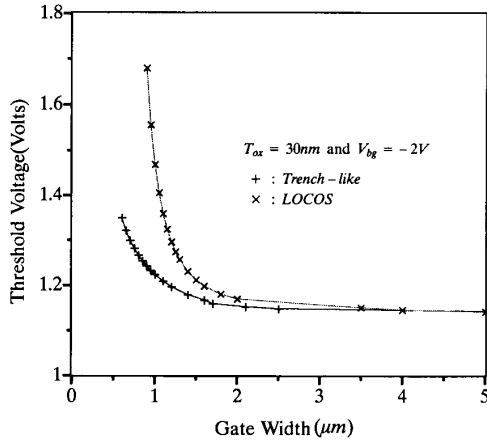


Fig. 5. Comparisons of the threshold voltage versus the effective gate width for different isolation structures of a MOSFET.

Trench-like are shown in Fig. 4(a) and (b), respectively, in which one half of the grids are used in the simulation due to the symmetry of the device structure. It must be noted that the orthogonality of the finite-box is kept, as shown in Fig. 4(a) and (b). The isolation structures are basically formed by two regions (layers): the semiconductor bulk and the insulator layer, in which the semiconductor bulk is covered by the insulator layer and the insulator layer has a transition region between field oxide and gate oxide. The hypertangent function can be used to describe these transitions. For a LOCOS structure, the shape functions for $f_0(\mu)$, $f_1(\mu)$, and $f_2(\mu)$ can be approximated by:

$$f_0(\mu) = -0.2425 + 0.2125 \tanh\left(\frac{\mu - 0.8}{0.2}\right) \quad (21a)$$

$$f_1(\mu) = 0.2125 - 0.2125 \tanh\left(\frac{\mu - 0.8}{0.2}\right) \quad (21b)$$

$$f_2(\mu) = 3. \quad (21c)$$

Similarly, for a Trench-like structure, we may write:

$$f_0(\mu) = -.08 + 0.05 \tanh\left(\frac{\mu - 0.8}{0.1}\right) \quad (22a)$$

$$f_1(\mu) = 0.375 - 0.375 \tanh\left(\frac{\mu - 0.8}{0.1}\right) \quad (22b)$$

$$f_2(\mu) = 3. \quad (22c)$$

The thicknesses of gate oxide and field oxide for these structures are 300 and 8500 Å, respectively. Note that the nonplanarity of the Trench-like structure is stronger than that of the LOCOS structure. The calculated threshold voltage versus the effective gate width for different isolation structures is shown in Fig. 5. It is clearly seen that the narrow-width effect in a Trench-like isolation structure is superior to that in a LOCOS isolation structure.

The coefficients of Fourier series (A_m and B_m) versus integer m used in the transformation for the oxide region

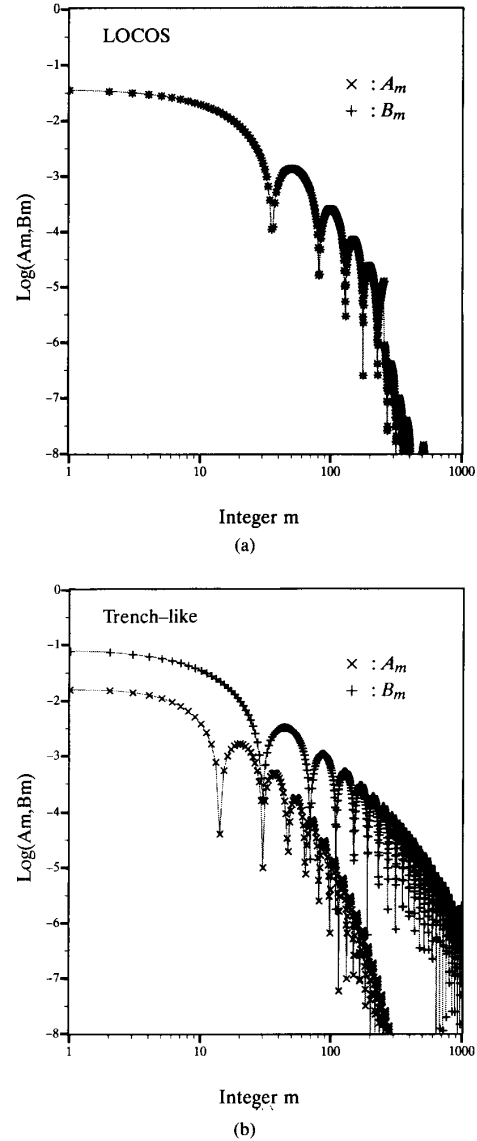


Fig. 6. The logarithmic plot of Fourier coefficients (A_m , B_m) versus integer m for the transformation of the oxide region: (a) LOCOS structure and (b) Trench-like structure.

of LOCOS and Trench-like structures are shown in Fig. 6(a) and (b). A_m is equal to B_m for the LOCOS structure due to the symmetry of the shape functions $f_0(\mu)$ and $f_1(\mu)$. Note that the convergence of Fourier series is $O(e^{-n})$. It is clearly shown in Fig. 6(a) and (b) that the magnitude and convergence of the Fourier series are strongly dependent on the nonplanarity of the semiconductor surface. It is expected that more Fourier series terms must be used to minimize the truncation error for Fourier series with slow convergence. In order to meet the same convergence criterion, the number of Fourier series for the Trench-like isolation are larger than that for the LOCOS isolation due to the slow convergence of

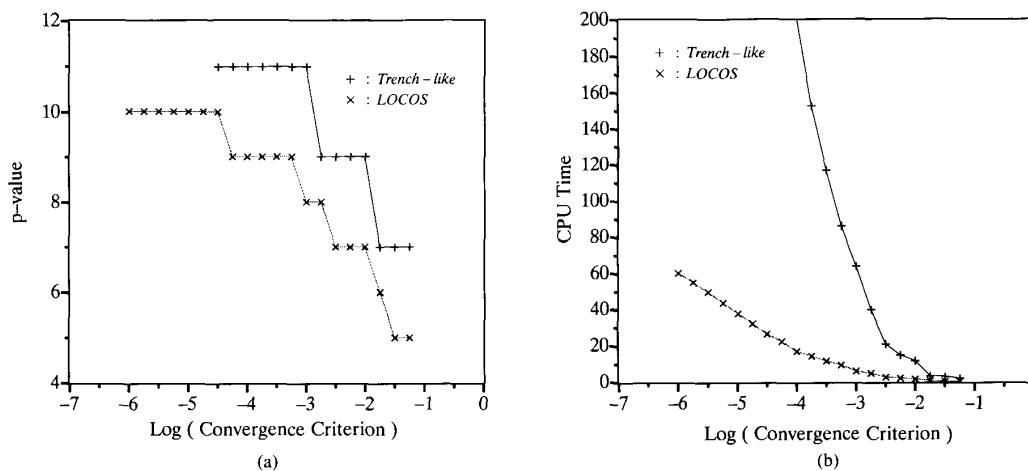


Fig. 7. (a) the p value and (b) the CPU time (s) versus the convergence criterion (Run by IBM RS/6000 model 320 workstation).

Fourier series for a Trench-like structure, as shown in Fig. 7(a). Besides, the convergence rate of the proposed nonlinear Jacobian iteration is dependent on the nonplanarity of the semiconductor surface. As a result, the CPU-time versus the convergence criterion for the transformation of the Trench-like structure is larger than that of the LOCOS structure, as shown in Fig. 7(b). Therefore, the computation efficiency will be deteriorated for the case with a strongly nonplanar semiconductor surface due to the slow convergence rate of both nonlinear Jacobian iteration and Fourier series.

The shape functions in (21)–(23) are only used to demonstrate the applications of the proposed method. Actually, the polynomial fitting method or other appropriate special function can be used to increase the accuracy of the shape function for the actual device structure.

V. CONCLUSIONS

A general analytical method to generate the grid structure for the nonplanar semiconductor surface is presented, in which the analytical formulation and the numerical algorithm are described in detail. The major advantage of the proposed method is that the discretized semiconductor device equations are invariant under the proposed coordinate transformation. It is demonstrated that the proposed method is efficient for the smooth semiconductor surface with mild nonplanarities, but the efficiency becomes deteriorated for the case with a strongly nonplanar semiconductor surface. Therefore, the proposed method is useful in improving the flexibility of conventional rectangular-based grid in handling the modern isolation device structures, such as modified LOCOS and Trench-like technologies.

ACKNOWLEDGMENT

Special thanks are given to Ms. G.-S. Hou for her helpful discussions.

REFERENCES

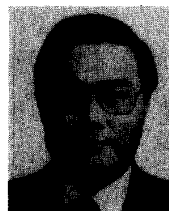
- [1] M. R. Pinto, C. S. Rafferty, and R. W. Dutton, "PISCES-II Poisson and continuity equation solver," Stanford Electronics Labs. Rep., Stanford Univ., CA, 1984.
- [2] G. Bacarani, R. Guerrieri, P. Ciampolini, and M. Rudan, "HFIELDS: A highly-flexible 2-D semiconductor devices analysis program," in *Proc. NASECODE IV Conf.*, pp. 3–12, 1985.
- [3] A. M. Winslow, "Numerical solution of the quasilinear Poisson's equation in a nonuniform triangle mesh," *J. Comput. Phys.*, vol. 2, pp. 149–172, 1967.
- [4] J. U. Brackbill and J. S. Saltzman, "Adaptive zoning for singular problems in two dimensions," *J. Comput. Phys.*, vol. 46, pp. 342–368, 1982.
- [5] Z. M. V.-Kovacs and M. Rudan, "Boundary fitted coordinate generation for device analysis on composite and complicated geometries," *IEEE Trans. Computer-Aided Design*, vol. 10, pp. 1242–1250, 1991.
- [6] P. Ciampolini, A. Forghieri, A. Pierantoni, A. Gnudi, M. V. Rudan, and G. Bacarani, "Adaptive mesh generation preserving the quality of the initial grid," *IEEE Trans. Computer-Aided Design*, vol. 8, pp. 490–500, 1989.
- [7] A. Seidl and M. Svoboda, "Numerical conformal mapping for treatment of geometry problems in process simulation," *IEEE Trans. Electron Devices*, vol. ED-32, pp. 1960–1963, 1985.



Shan-Ping Chin (S'86) received the B.S. degree from the Department of Physics, National Tsing-Hua University, Taiwan, Republic of China, in 1985, and the Ph.D. degree from the Institute of Electronics, National Chiao-Tung University, in 1992.

His research interests are in the device modeling of deep submicrometer MESFET's. He joined the Electronics Research and Service Organization (ERSO), ITRI, Taiwan, in 1992. His present interests focus on semiconductor device and IC

process simulation for VLSI.



Ching-Yuan Wu (M'72) received the B.S. degree in electrical engineering from National Taiwan University, Taiwan, Republic of China, in 1968, and the M.S. and Ph.D. degrees from the State University of New York (SUNY) at Stony Brook, in 1970 and 1972, respectively.

During the 1972–1973 academic year he was appointed as a Lecturer at the Department of Electrical Sciences, SUNY, Stony Brook. During the 1973–1975 academic years, he was a Visiting Associate Professor at National Chiao-Tung Univer-

sity (NCTU), Taiwan. In 1976, he became a Full Professor in the Department of Electronics and the Institute of Electronics, NCTU where he had been the Director of Engineering Laboratories and Semiconductor Research Center during 1974–1980; the Director of the Institute of Electronics, during 1978–1984; and Dean, College of Engineering, during 1984–1990. He was a principal investigator of the National Electronics Mass Plan—Semiconductor Devices and Integrated—Circuit Technologies during 1976–1979, and had been a Coordinator of the National Microelectronics Researches and High-Level Man-Power Education Committee, National Science Council, Republic of China, during 1982–1988. He has been the Research Consultant of the Electronics Research and Service Organization (ERSO), ITRI; a member of the Academic Review Committee, the Ministry of Education; and the chairman of the Technical Review Committee on Information and Microelectronics Technologies, the Ministry of Economic Affairs. His research activities have been in semiconductor device physics and modelings, integrated—circuit designs and technologies.

His present research areas focus on the developments of efficient 2-D and 3-D simulators for deep-submicrometer semiconductor devices, design rules and optimization techniques for deep-submicrometer CMOS devices, and key technologies for deep-submicrometer CMOS devices. He has published over 150 papers in the semiconductor field and has served as a reviewer for international journals such as *IEEE ELECTRON DEVICE LETTERS*, *IEEE TRANS. ON ELECTRON DEVICES*, and *Solid-State Electronics*.

Dr. Wu is a member of the Honorary Editorial Advisory Board of Solid-State Electronics and is a board member of the Chinese Engineering Society. He received the Academic Research Award in Engineering from the Ministry of Education (MOE), in 1979; the outstanding Scholar award from the Chinese Educational and Cultural Foundation, in 1985. He has received the outstanding research Professor fellowship from the Ministry of Education and the National Science Council (NSC), Republic of China, during 1982–1993.